Temperature dependence of optical properties on BaTiO₃ thin films for optoelectronics applications

R. SENGODAN[a], B. CHANDAR SHEKAR[b*], R. BALAMURUGAN[a], R. KANNAN[a], R. RANJITHKUMAR[c]

[a]Department of Physics, Kumaraguru College of Technology, Coimbatore – 641049,
Tamil Nadu. India
[b] Departments of Physics, Kongunadu Arts and Science College, G.N- Mills,
Coimbatore – 641029, Tamil Nadu, India
[c]KIRND Institute of Research and Development, Thiruchirapalli, Tamilnadu, India

Barium titanate nano particles were synthesized by the wet chemical method using the starting materials barium chloride ($BaCl_2$), titanium dioxide (TiO_2) and oxalic acid with different calcinations temperatures. The prepared nano particles were thermally grown onto well cleaned glass substrates under the vacuum of 10^{-5} torr, using 12A4 Hind Hivac coating unit. The thickness of the film was measured by quartz crystal monitor. The composition of nanoparticles and thin films were identified by EDS spectrum. From X-ray analysis, it has been found that BaTiO₃ nanoparticles possess tetragonal structure and the deposited films were polycrystalline in nature, whereas the crytstallinity increases with increase of annealing temperature. Absorption coefficient, extinction coefficient, optical band gap and refractive index of films were estimated from optical transmittance spectrum. The extinction coefficient and refractive index of the BaTiO₃ thin films increases with increasing annealing temperature. The optical band gap energy value decreases with increase of annealing temperature.
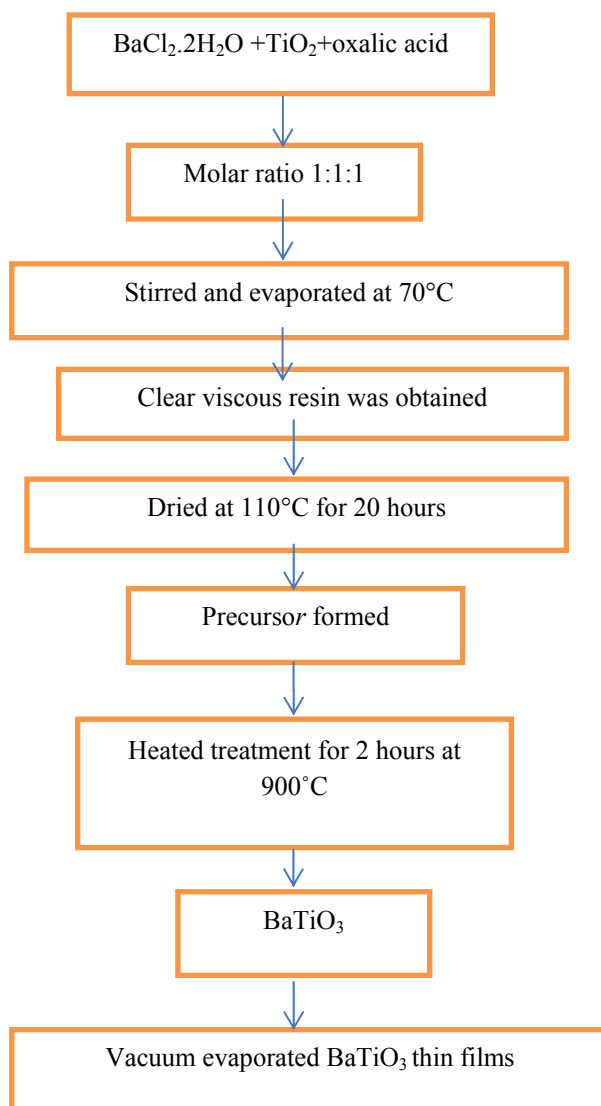
1. Introduction

Barium titanate (BT) is one of the most important ceramics due to its outstanding dielectric and ferroelectric properties with different applications such as multilayer capacitors, thermistors and electric devices [1]. Thin films of barium titanate with perovskite crystal structure are known as one of the key materials for use in the solid-state devices including capacitors, memories, thermistors, sensors and actuators [2, 3]. Barium titanate with high transmittance in the visible wavelength region (380–760 nm) is a suitable material for various electro-optic applications. During last decade most of the experimental work carried out so far relate to preparation of BaTiO₃ thin films like electrochemical deposition [4], sputtering [5], plasma evaporation [6], hydrothermal [7], solvothermal [8], pulsed laser ablation [9] and sol-gel [10, 11]. In our previous work, we reported thicknesses dependence on BaTiO₃ thin films in order to improve their optical and dielectric properties by vacuum evaporation method [12, 13]. Hence, the vacuum evaporation was considered as one of the most prominent because of the advantages of low cost and uniform deposition on substrates. To the best our knowledge no work has been report on as grown and annealing effect on BaTiO₃ thin films prepared by vacuum evaporation method. The elemental, structure, morphology and optical properties of BaTiO₃ thin films have been thoroughly characterized by using various techniques for both as grown and annealed films.

The variation annealing temperature can provide more details on the behaviour of changes and ability to enhance the optical properties. Elemental, structure, morphology and optical properties such as transmittance, absorption coefficient, extinction coefficient, band gap energy and refractive index were studied and are discussed in detail.

2. Experimental Details

2.1. Synthesis of BaTiO₃ nanoparticles

BaTiO₃ nanoparticles were synthesized by using Wet chemical method. The starting materials used were barium chloride ($BaCl_2.2H_2O$), Titanium dioxide (TiO_2) powder and Oxalic acid. The solution of barium chloride, titanium dioxide and Oxalic acid mole ratio1: 1: 1 was stirred and evaporated at 70°C till a clear, viscous resin was obtained, then dried at 110° C for 20 hours. The precursor formed was heated at 900° C for 2 hours and was brought to the room temperature to form BaTiO₃ nanoparticles.

```
                    ┌─────────────────────────────────────┐
                    │  BaCl₂.2H₂O +TiO₂+oxalic acid        │
                    └─────────────────────────────────────┘
                                     ↓
                    ┌─────────────────────────────────────┐
                    │         Molar ratio 1:1:1           │
                    └─────────────────────────────────────┘
                                     ↓
                    ┌─────────────────────────────────────┐
                    │     Stirred and evaporated at 70°C   │
                    └─────────────────────────────────────┘
                                     ↓
                    ┌─────────────────────────────────────┐
                    │     Clear viscous resin was obtained │
                    └─────────────────────────────────────┘
                                     ↓
                    ┌─────────────────────────────────────┐
                    │     Dried at 110°C for 20 hours      │
                    └─────────────────────────────────────┘
                                     ↓
                    ┌─────────────────────────────────────┐
                    │         Precursor formed             │
                    └─────────────────────────────────────┘
                                     ↓
                    ┌─────────────────────────────────────┐
                    │   Heated treatment for 2 hours at    │
                    │              900˚C                   │
                    └─────────────────────────────────────┘
                                     ↓
                    ┌─────────────────────────────────────┐
                    │              BaTiO₃                  │
                    └─────────────────────────────────────┘
                                     ↓
                    ┌─────────────────────────────────────┐
                    │  Vacuum evaporated BaTiO₃ thin films │
                    └─────────────────────────────────────┘
```

2.2. BaTiO$_3$ thin film preparation

The prepared nano particles of BaTiO$_3$ placed in the molybdenum boat (200 amps) and get heated with high current by energizing transformer. The transformer capable of supplying 150 amperes at 20 volts is used to provide the necessary current for heating the molybdenum source. Prior to evaporation, the evaporant material was carefully degassed at a lower temperature for about thirty minutes with the shutter closed. Deposition of the material on to pre-cleaned glass substrates under the pressure of about 10^{-5} Torr was achieved by slowly varying the current. A constant rate of evaporation 1Å/sec was maintained throughout the film preparation. The scratch test revealed that adhesion of the films to the substrate seems to be extremely good.

The substrate to source distance was optimized to be at 0.175 m and source to crystal distance was optimized to be at 0.21 m inside the vacuum chamber. The as deposited thin films and annealed films at different temperatures for 1 h were used to study the structure, morphology and optical properties.

2.3. Measurements

Thickness of the films was measured through quartz crystal monitor ("Hind Hivac" Digital Thickness Monitor Model–DTM– 101). The structural aspects of the films were analyzed, using X-ray diffractometer with filtered CuKα radiation (λ = 1.5418 Å). The surface morphology of the films was examined by scanning electron microscope (SEM) and the high-resolution transmission electron microscopy (HRTEM). The optical studies were carried out by using JASCO – UV/VISIBLE spectrophotometer (JASCO V – 670, Japan).

3. Result and discussion

3.1. EDS Analysis

Fig. 1 shows the EDS spectrum of as prepared BaTiO₃ nanoparticles and as deposited and annealed at different temperature of BaTiO₃ thin film of thicknesses 150 nm. Elemental composition analysis indicated the presence of Ba, Ti and O in the synthesized BaTiO₃nanoparticles as well as in the deposited and annealed BaTiO₃ thin films.
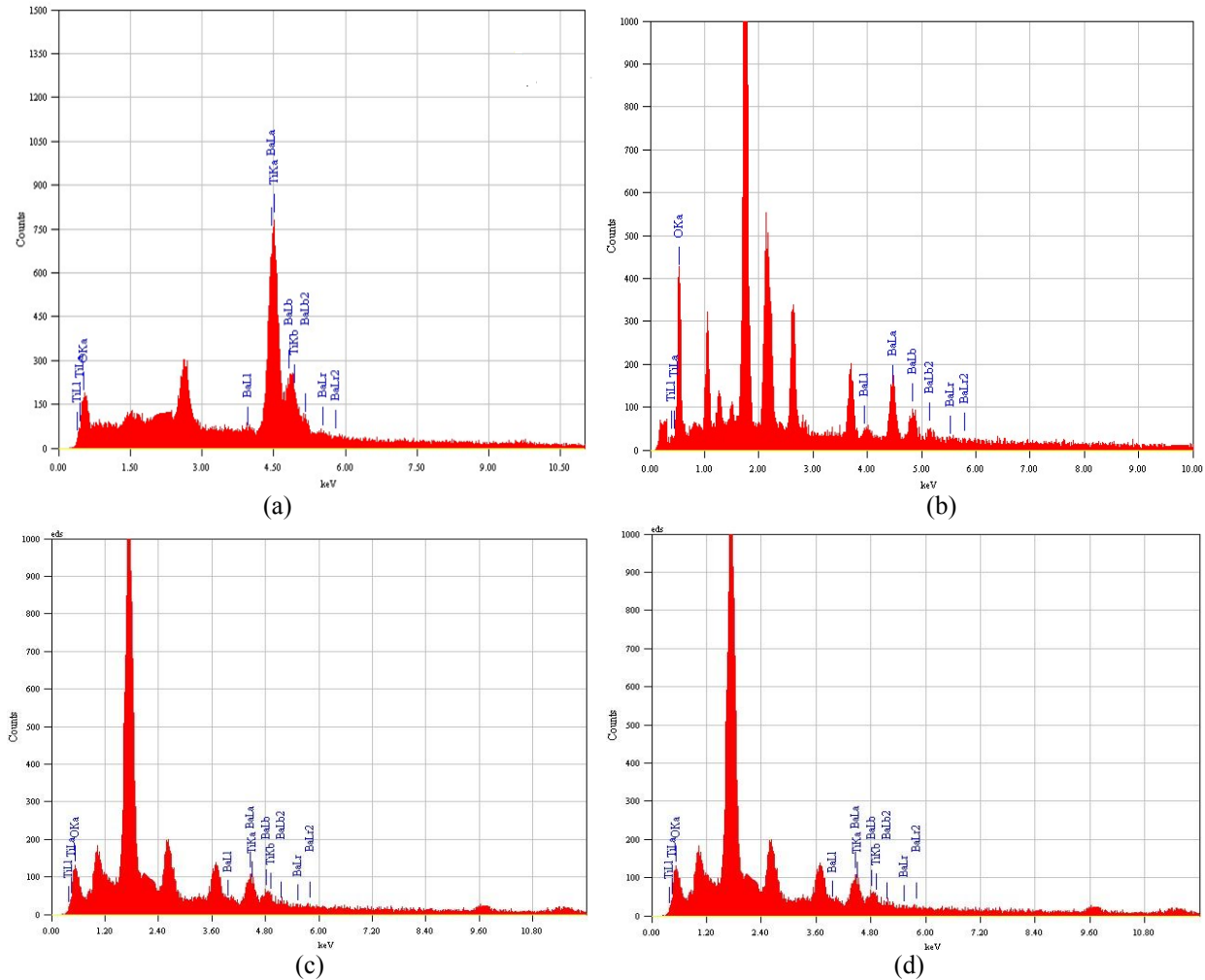

Fig. 1. EDS spectrum of (a) BaTiO₃ nanoparticles (b) BaTiO₃ thin films of thickness 150 nm as deposited (c) BaTiO₃ thin films annealed at 473 K(d) BaTiO₃ thin films annealed at 673 K

3.2. Surface Morphology

3.2.1. Scanning Electron Microscope (SEM) Studies

Fig. 2. shows the SEM images of BaTiO₃ particles. Rod like and uniform grain size are distributed throughout the particles. Fig 2 (b,c and d) shows the SEM images of as deposited and annealed BaTiO₃ thin films of thickness 150 nm. SEM image showed the grains are uniformly distributed. The grain size of the films increases with increasing annealing temperature. Increase in grain size upon annealing leads to decrease of grain boundary scattering [14]. The obtained smooth surface having grain size in the micrometer scale range for as deposited and annealed thin films indicated the feasibility of utilizing them in optoelectronic device applications.
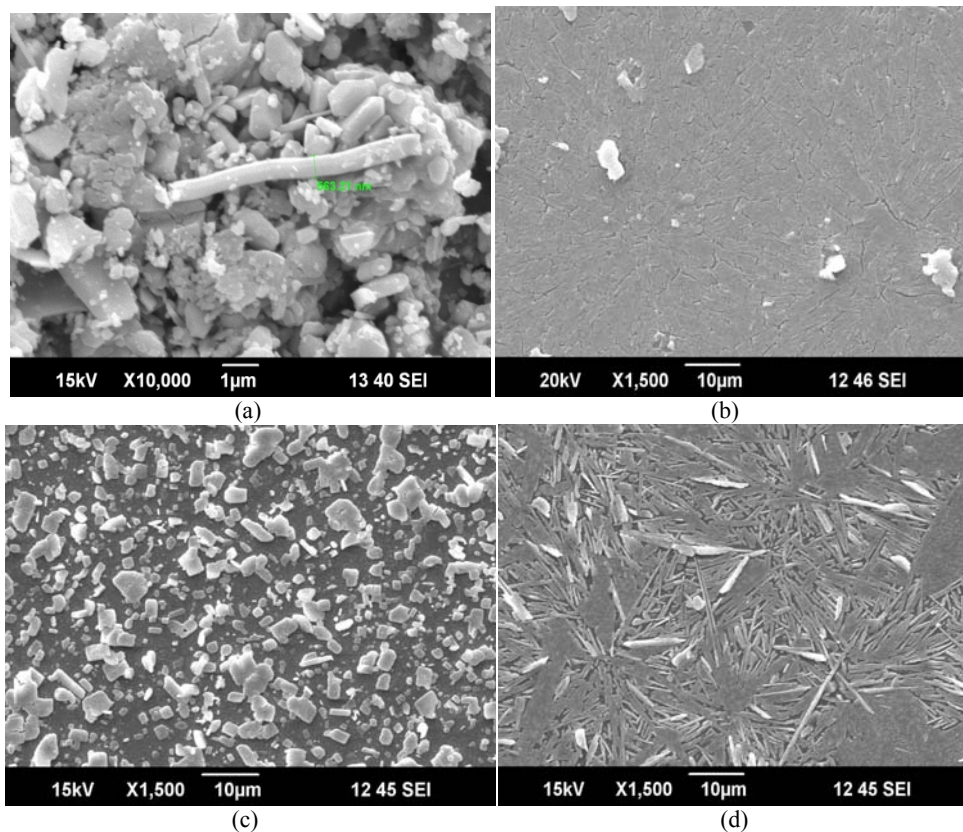
Fig. 2. SEM images of (a) BaTiO₃ nanoparticles (b) BaTiO₃ thin films of thickness 150 nm as deposited
(c) BaTiO₃ thin films annealed at 473 K(d) BaTiO₃ thin films annealed at 673 K

3.2.2. Transmission Electron Microscope (TEM)

Fig. 3 shows the HRTEM micrography of the $BaTiO_3$ nanoparticles. It is observed that particles had nano rod like shape. The diameter of the nano rod was less than 100 nm. Similar type of nano rods had been observed by earlier investigators [15, 16].

Fig.4 shows the selected area electron diffraction (SAED) pattern of $BaTiO_3$ nanoparticles. The circular bright continuous rings in the SAED pattern corroborate the fact that particles were nano sized and confirmed the crystalline nature of nanoparticles.
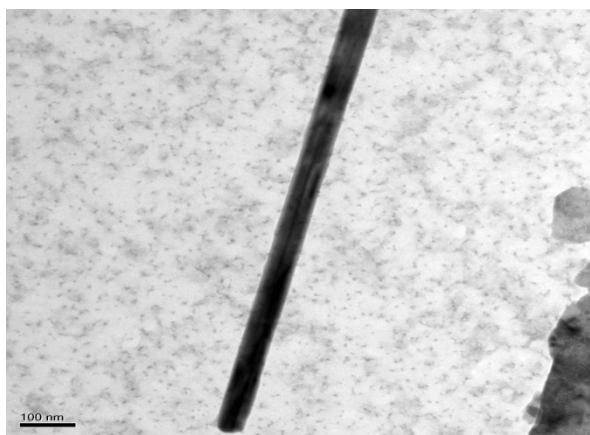
Fig. 4. SAED pattern of BaTiO₃ nanoparticles

Fig.3. HRTEM micrography of the BaTiO₃ nanoparticles
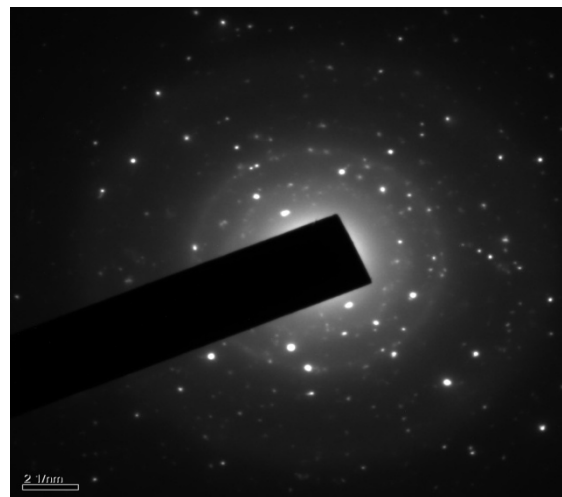
3.3. X – Ray Diffraction Analysis

Fig. 5 shows the XRD pattern of $BaTiO_3$ nanoparticles. From XRD measurement, the particle is exhibited to the tetragonal structure. The crystallite size was calculated using scherrer's formula at different diffraction angles and tabulated in the Table 1. From the table it is observed that crystallite size is varies between 41.65 nm to 59.56 nm.

The crystallite size [17] is calculated from the Scherrer's formula from the full with half – maximum of the XRD peaks

$$D = 0.94\lambda/\beta\cos\theta \qquad (1)$$

Where λ is the wavelength of the X-rays used, 2θ is the angle between the incident and scattered X-rays and β is the full width at half maximum. The strain (ϵ) is calculated from the formula

$$\epsilon = \beta\cos\theta/4 \qquad (2)$$

The dislocation density (δ) is defined as the length of dislocation lines per unit volume of the crystal and is given by

$$\delta = 1/D^2 \qquad (3)$$
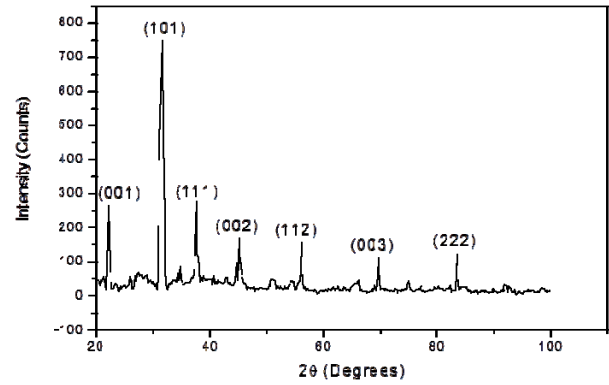
Fig. 5. XRD pattern of BaTiO₃ nanoparticles

Table 1. Structural parameter of BaTiO₃ nanoparticles

Temperature (°C)	Calculated values			Standard values (JCPDS-ICCD)			Crystallite size
	2θ (Degrees)	d(Å)	h k l	2θ (Degrees)	d(Å)	h k l	(nm)
900	22.154	4.0093	001	22.237	3.9820	001	43.45
	31.570	2.832	101	31.495	2.8280	101	57.04
	38.942	2.311	111	38.894	2.306	111	43.27
	44.939	2.015	002	44.909	2.008	002	41.65
	56.002	1.641	112	55.980	1.635	112	59.56
	69.97	1.343	003	69.909	1.339	003	52.97
	83.557	1.156	222	79.437	1.202	222	58.92

XRD pattern of as deposited BaTiO₃ thin films of thickness 150 nm and film annealed at 473K and 673K for 1h are shown in fig 6. The XRD patterns show that the films were polycrystalline in nature. As the annealing temperature increases, the peaks in the XRD patterns become more sharp and intense indicating better crystallinity. The peak splitting observed for both as deposited and annealed BaTiO₃ thin films indicates the tetragonal structure [18, 19].
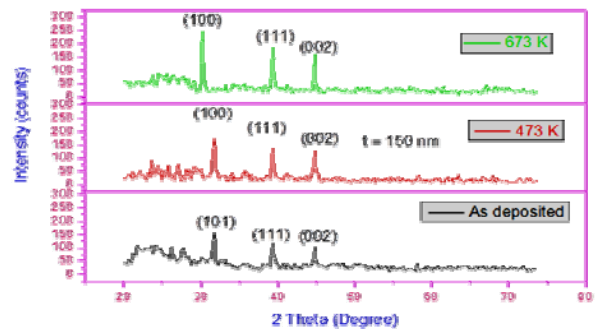
Fig. 6. XRD pattern of as deposited and annealed BaTiO₃ thin films (at 673 and 473K) of thickness 150 nm

Table 2. Structural parameter of BaTiO₃ thin films of thickness 150 nm at different annealed temperature

Annealing temperature (°C)	2θ (Degrees)	hkl	Crystallite size (nm)	Strain (ε) x10⁻³ (lin⁻²m⁻⁴)	Dislocation density (δ) x10⁻⁵ (lin/m²)
As deposited	31.69	101	28.89	1.237	1.198
	38.66	111	23.14	1.465	1.867
	44.78	002	20.87	1.625	2.295
200	31.69	101	32.38	1.131	0.953
	38.66	111	25.36	1.371	1.554
	44.78	002	24.16	1.455	1.713
400	31.69	101	36.73	1.069	0.741
	38.66	111	27.54	1.273	1.318
	44.78	002	26.12	1.342	1.465

The crystallite size, strain and dislocation density of as deposited BaTiO₃ thin film of thickness 165 nm and film annealed at different temperatures are presented in table 2. From the table it is seen that the crystallite size increase slightly with increase of annealing temperature whereas the strain and dislocation density decreases with increase in annealing temperature. The decrease in the strain and dislocation density indicates the formation of higher quality films at higher annealing temperatures [20].

3.4. Optical studies

The transmittance spectra for BaTiO₃ thin film of thicknesses 150 nm annealed at various temperatures are shown in figure 7. It is observed that transmittance decreases with increase in annealing temperatures. The average transmittance in the visible region is 74%. The higher transmittance observed in the film at higher wavelength region is attributed to less scattering effects, structural homogeneity and better crystallanity, whereas the lower transmittance might be due to the less crystallanity leading to more light scattering [21].
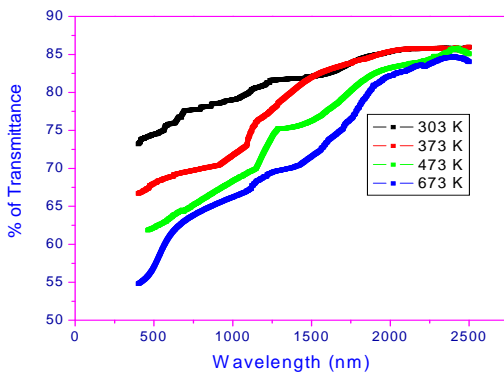

Fig. 7. Transmittance spectra for BaTiO₃ thin film of thicknesses 150 nm annealed at various temperatures

In order to describe the fundamental absorption edge, the spectral dependence of absorption coefficient (α) is directly determined using the relation,

$$\alpha = \frac{4\pi k_f}{\lambda} \tag{4}$$

Where λ is the wavelength of the incident radiation and k_f is the extinction coefficient. 11

The extinction coefficient is defined as,

$$k_f = \frac{2.303 \log_{10}\left(\frac{1}{T}\right)\lambda}{4\pi t} \tag{5}$$

Where 't' is film thickness. The nature of transition can be investigated on the basis of dependence of α on the photon energy $h\upsilon$. For direct and allowed transitions, the theory of fundamental absorption leads to the following photon energy dependence near the absorption edge as,

$$\alpha \propto \left[h\upsilon - E_g\right]^m \tag{6}$$

where $h\upsilon$ and E_g are the photon energy and the optical energy gap respectively. In this expression, the values of m are $\frac{1}{2}$ and 2 for direct and indirect transition respectively.

The optical properties of any material are characterized by two parameters n and k_f. The plot of transmission T against wavelength λ is found to vary as [22]

$$T = \frac{16n_a n_g n^2 \exp(-\alpha t)}{R_1^2 + R_2^2 \exp(-2\alpha t) + 2R_1 R_2 \exp(-\alpha t)\cos(4\pi nt/\lambda)} \tag{7}$$

Where,

$$R_1 = (n+n_a)(n_g+n)$$

$$R_2 = (n-n_a)(n_g-n)$$

α is the absorption coefficient and n, n_a, n_g are the refractive indices of the film, air and substrate respectively. Iterations were carried out till the desired convergence was achieved.

The porosity (ρ) values (Volume of pores per volume of film) of the films were calculated using the relation [23]

$$\rho = 1 - \frac{n_f^2 - 1}{n_b^2 - 1} X100 \qquad (8)$$

Fig. 8 shows the variation of k_f with wavelength for BaTiO₃ thin films of thickness 150 nm for different annealing temperatures. The extinction coefficient increases with increase in annealing temperature. This seems to originate from the fact that at higher annealing temperature the crystal size of the film increases. The calculated extinction coefficient (k_f) value actually includes the total optical losses caused by absorption and scattering [24]. At high annealing temperature, crystalline size is large; this would cause fairly strong scattering loss. This is accounted in the calculation of k_f, thus resulting in the high value of k_f at higher annealing temperature.
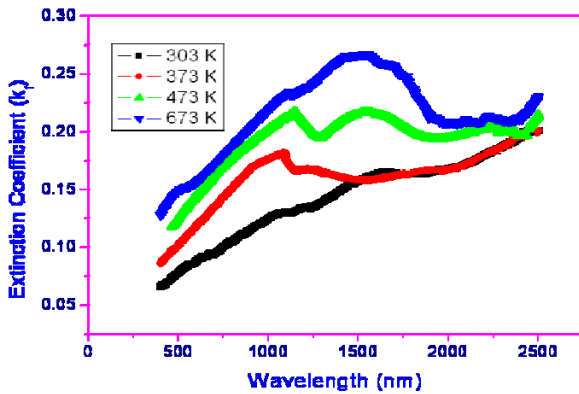

Fig. 8. Variation of k_f with wavelength for BaTiO₃ thin films of thickness 150 nm for different annealing temperatures

Fig. 9 shows the variation of absorption coefficient (α) with wavelength for BaTiO₃ films of thickness 150 nm for different annealing temperatures. It is seen that absorption coefficient increases with increase in annealing temperature. From the absorption coefficient the band gap

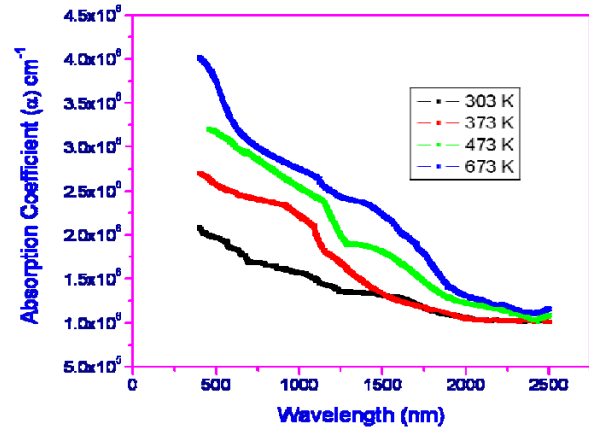energy of the annealed films were calculated by using the equation (6).

Fig. 9. Variation of absorption coefficient (α) with wavelength for BaTiO₃ films of thickness 150 nm for different annealing temperatures

Fig. 10 shows the variation of $(\alpha h\upsilon)^2$ versus photon energy for BaTiO₃ thin film of thickness 150 nm for different annealing temperatures. The dependence of optical band gap with different annealing temperature is given in the table 3. It is observed that direct band gap decreases with increase in the annealing temperatures. The decrease in band gap can occur due to several factors such as the crystallite size effect, decreases in strain and stress in the films. Similar observations are made by L. V. Maneeshya et al [25] for BaTiO₃ thin films.

Table. 3. Temperature dependence on optical band gap of BaTiO₃ thin films of thickness 150 nm at different annealed temperature

Annealing temperature (K)	Band gap energy (eV)
303	3.906
373	3.894
473	3.882
673	3.860

Table 4 shows the porosity of the BaTiO₃ thin film of thickness 150 nm annealed at different temperatures. It is observed that porosity decreases with increase in annealing temperature.
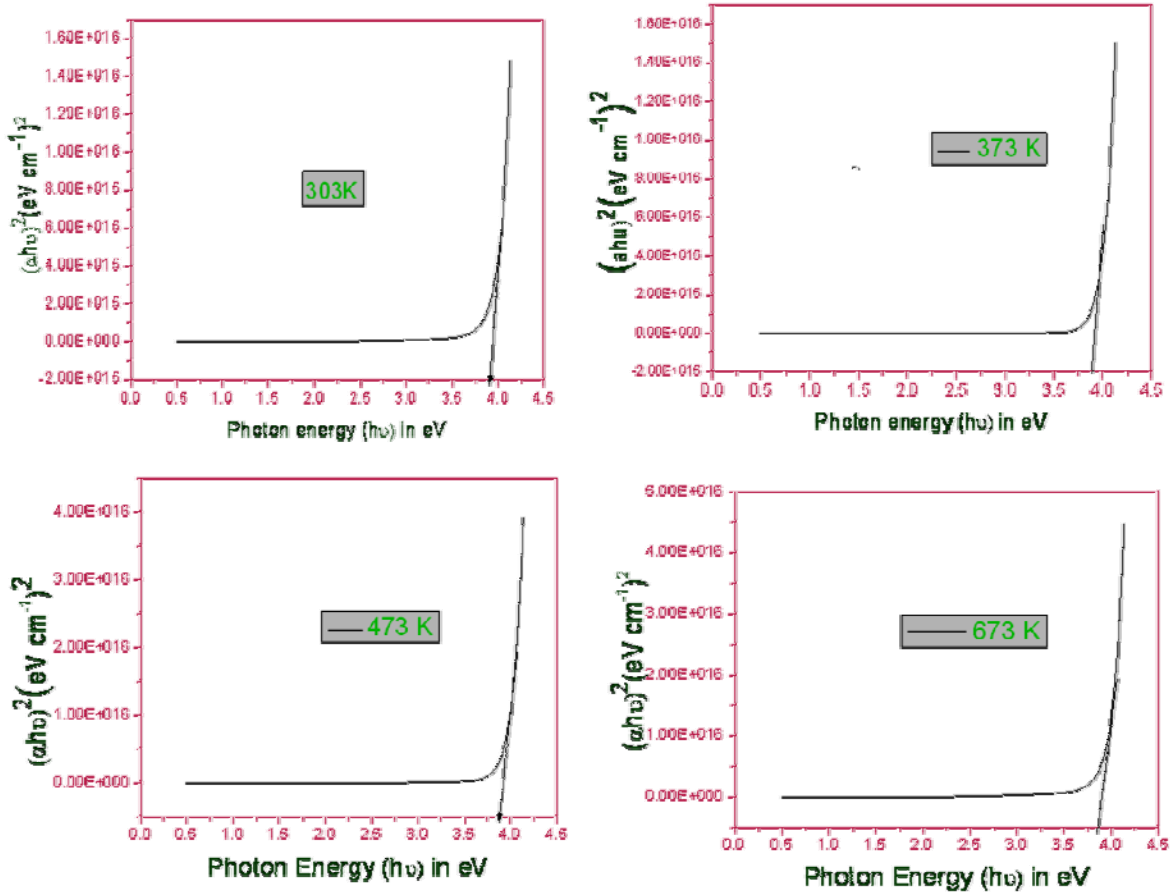
Fig. 10. Variation of $(\alpha h\upsilon)^2$ versus photon energy for BaTiO₃ thin film of thickness 150 nm
for different annealing temperatures

Table. 4. Porosity of the BaTiO₃ thin film of thickness
150 nm annealed at different
temperature

Temperature (K)	Porosity (ρ) %
303	42.7
373	42.35
473	32.8
673	23.2

Fig. 11. Variation of refractive index with wavelength
for BaTiO₃ thin film of thickness 150 nm at different
annealing temperatures

Fig. 11 shows the refractive index with wavelength for BaTiO₃ thin films of thickness 150 nm for different annealing temperatures. It is observed that refractive index of the BaTiO₃ film increases with annealing temperature. The refractive index of the film is directly proportional to electronic polarization and is thus inversely proportional to the inter – atomic spacing. Therefore, reduction in the interatomic spacing resulting in the densification of the film (porosity reduction) will lead to an increase in the refractive index [26].
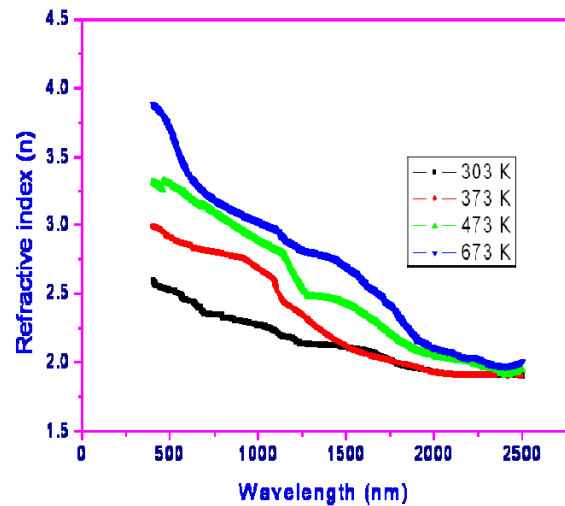
4. Conclusion

We have successfully synthesized BaTiO₃ nanoparticles by wet chemical method using commercially

available chemicals such as BaCl$_2$, TiO$_2$ and oxalic acid. The prepared nanopowders were thermally grown onto well cleaned glass substrates by vacuum evaporation method. X-ray analysis showed that particle has a tetragonal nature and the deposited film has a polycrystalline nature, whereas crystallinity increases with increase in annealing temperature. The extinction coefficient and refractive index of the BaTiO$_3$ thin films increases with increasing annealing temperature. The band gap energy decreases from 3.906 to 3.860 with increasing annealing temperature.

References

[1] R. Ashiri, Ali Nemati, M. Sasani Ghamsari, H. Aadelkhani, Journal of Non-Crystalline Solids **355**, 2480 (2009).

[2] Raja Sengodan, Bellan Chandar Shekar, Sugumaran Sathish, Optik **125**, 4819 (2014).

[3] R. Thomas, D.C. Dube, M.N. Kamalasanan, S. Chandra, Thin Solid Films **21**, 346 (1999).

[4] C.T. Wu, F.H. Lu, Thin Solid Films **398&399**, 621 (2001).

[5] L. V. Maneeshya, V. S. Anitha, V. Thomas, K. Joy, J. Mater Sci: Mater Electron **26**, 2947 (2015).

[6] H. Huang, X. Yao, Ceram. Int. **30**, 1535 (2004).

[7] C. K. Tan, G. K. L. Goh, G. K. Lau, Thin Solid Films **516**, 5545 (2008).

[8] C. K. Tan, G. K. L. Goh, Thin Solid Films **515**, 6572(2007).

[9] P. Bhattacharya, T. Komeda, D. Park, Y. Nishioka, J. Appl. Phys **32**, 4103 (1993).

[10] Y. Huang, J. Lin, H. Du, L. Gao, Y. Hu, Mater. Lett **60**, 3818 (2006).

[11] R. Ashiri, Ali Nemati, M. Sasani Ghamsari, Sanjabi, M. Aalipour, Materials Research Bulletin **46**, 2291 (2011).

[12] R. Sengodan, B. Chandar Shekar, S. Sathish, J. Optoelectron. Adv. M. **14**, 653 (2012).

[13] R. Sengodan B. Chandar Shekar, S. Sathish, J. Nanoelectron. Optoelectron. **8**, 1 (2013).

[14] Sathish Sugumaran, Chandar Shekar Bellan, Dinesh Muthu, Sengodan Raja, Dinesh Bheeman, Ranjithkumar Rajamani, RSC Adv **5**, 10599 (2015).

[15] J. J. Urban, W. S. Yun, Q. Gu, H. Park, J. Am. Chem. Soc. **124**, 1186 (2002).

[16] C. Liu, B. Zou, A. J. Rondinone, Z. J. Zhang, J. Am. Chem. Soc. **123**, 4344 (2001).

[17] R. Kannan, S. Ganesan, T. M. Selvakumari, Digest Journal of Nanomaterials and Biostructures **7**, 1039 (2012).

[18] E. J. H. Lee, F. M. Pontes, E. R. Leite, E. Longo, J. A. Varela, E. B. Araujo, J. A. Eiras, J. Mater. Sci. Lett. **19**, 1457 (2000).

[19] E. J. H. Lee, F. M. Pontes, E. R. Leite, E. Longo, R. Magnani, P. S. Pizani, J. A. Varela, Mater. Lett. **58**, 1715 (2004).

[20] M. Tomisu, N. Inoue, Y. Yasuoka, Vacuum **47**, 239 (1996).

[21] E. M. Bachari, G. Baud, S. Ben Amor, M. Jacquet, Thin Solid Films **348**, 165 (1999).

[22] J. C. Manifacier, J. Gasiot, J. P. Fillard, J. Phys. E **9**, 1002 (1976).

[23] B. E. Yoldas, P. W. Partlow, Thin Solid Films **129**, 1 (1985).

[24] R. Thomas, D. C. Dube, M. N. Kamalasanan, S. Chandra, Thin Solid Films **346**, 212 (1999).

[25] L.V. Mahneeshya, V. S. Anitha, S. S. Lekshmy, L. John Berlin, P. B. Nair, G. P. Daniel, P. V. Thomas, K. Joy, J. Mater Sci: Mater Electron. **24**, 848 (2013).

[26] C. B. Samantaray, A. Dhar, D. Bhattacharya, M. L. Mukherjee, S. K. Ray, J Mater Sci: Mater Electron **12**, 365 (2001).

*Corresponding author chandar.bellan@gmail.com